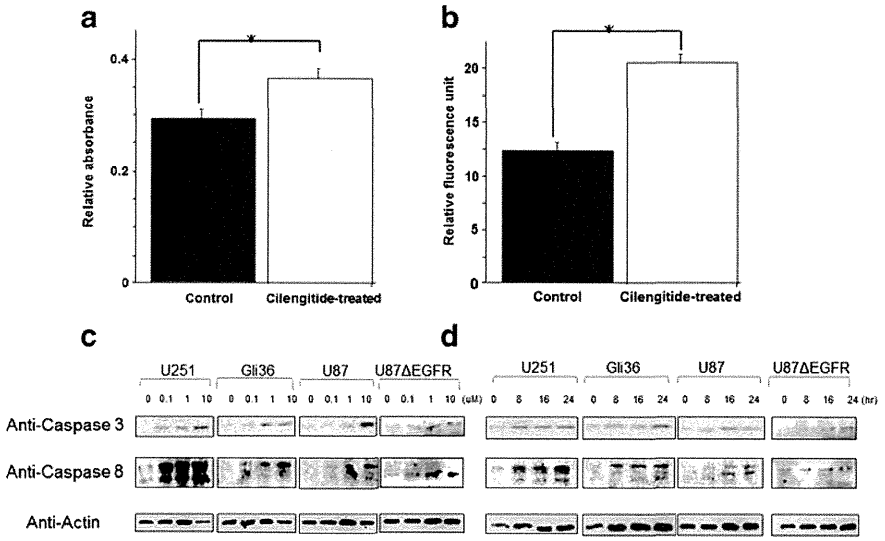

Figure 3 QRT-PCR analysis and activation of caspase-3/7 and -8 in cilengitide-treated cells. U87ΔEGFR cells were treated with 0.5 μM cilengitide for 16 h with the colorimetric protease assay kit. For the activity of caspase-8, the relative absorbance (RA) of U87ΔEGFR cell clusters were higher than control (0.27 ± 0.01 RA vs. 0.36 ± 0.01 RA, respectively; $P < 0.05$) (**a**). Cilengitide-induced apoptosis was also detected with the CellEvent™ Caspase-3/7 Green Detection Reagent. The RFU of U87ΔEGFR cell clusters were higher than control (35.4 ± 0.78 RFU vs. 16.5 ± 0.5 RFU, respectively; $P < 0.05$) (**b**). Immunoblot analysis revealed that caspases 3 and 8 were processed in all examined cell lines following treatment with cilengitide in a concentration- (**c**) and time-dependent manner (**d**).

compared to control (35.4 ± 0.78 vs. 16.5 ± 0.5, respectively; $P < 0.05$) (Figure 4e).

Cilengitide induces apoptosis in U87ΔEGFR-derived xenografts

The effect of cilengitide on the induction of apoptosis was examined in U87ΔEGFR-derived xenografts. At 5 days after implantation, the rats were administered cilengitide (1 mg/500 μL PBS) 3 times/week intraperitoneally, and the rats were killed at 18 days after implantation. Caspase 8 gene expression was analyzed with QRT-PCR and the induction of apoptosis in frozen sections of the U87ΔEGFR xenografts was examined under a fluorescent microscope. QRT-PCR revealed a statistically significant 10.1-fold increase in caspase 8 gene expression in Cilengitide treated tumors compared with control tumors (Figure 4f). A subpopulation of apoptotic cells were visualized by TUNEL treatment using the In Situ Cell Death Detection Kit (apoptotic cells: TMR red; nuclei: DAPI, blue). The control sections exhibited a smaller amount of red fluorescent cells (Figure 4g), whereas more scattered red fluorescent cells were observed in the cilengitide-treated xenografts (Figure 4h). To quantify the cytotoxic effect of cilengitide, the number of apoptotic cells per high-power field (HPF) in U87ΔEGFR control xenografts and U87ΔEGFR cilengitide-treated xenografts were assessed (Figure 4i). The number of apoptotic cells in U87ΔEGFR cilengitide-treated xenografts (26.2 ± 3.8 cells/HPF) was significantly higher than in U87ΔEGFR control xenografts (1.40 ± 0.6 cells/HPF) ($P < 0.05$). The average percentage of apoptotic cells was 5% in U87ΔEGFR cilengitide-treated xenografts (Figure 4j).

Discussion

Cilengitide treatment induced morphological changes and cell detachment in glioma cells incubated in dishes and decreased cell viability in a dose and time-dependent manner. Microarray analysis showed that the expression of 265 genes was changed after cilengitide treatment. The expression of 214 genes was up-regulated 4-fold more and the expression of 51 genes was down-regulated to less than 25% of control and apoptotic signaling pathways were over-represented in the pathway analysis. In addition to the effect of cilengitide in cultured cells, cilengitide also induced apoptosis in U87ΔEGFR-derived xenografts, suggesting that the induction of apoptosis also occurs in vivo.

Cytotoxic effect of Cilengitide

Cilengitide is an angiogenesis inhibitor that targets the integrins αvβ3 and αvβ5, which bind to ECM proteins such as vitronectin and fibronectin (Burke et al. 2002; Albert et al. 2006). Because integrins are expressed in tumor cells and tumor endothelial cells (Varner & Cheresh 1996a), it is speculated that cilengitide can inhibit tumor growth by at least 2 mechanisms: by targeting the tumor cells directly and by inhibiting tumor angiogenesis (Tucker 2003; Oliveira-Ferrer et al. 2008; Chatterjee et al.

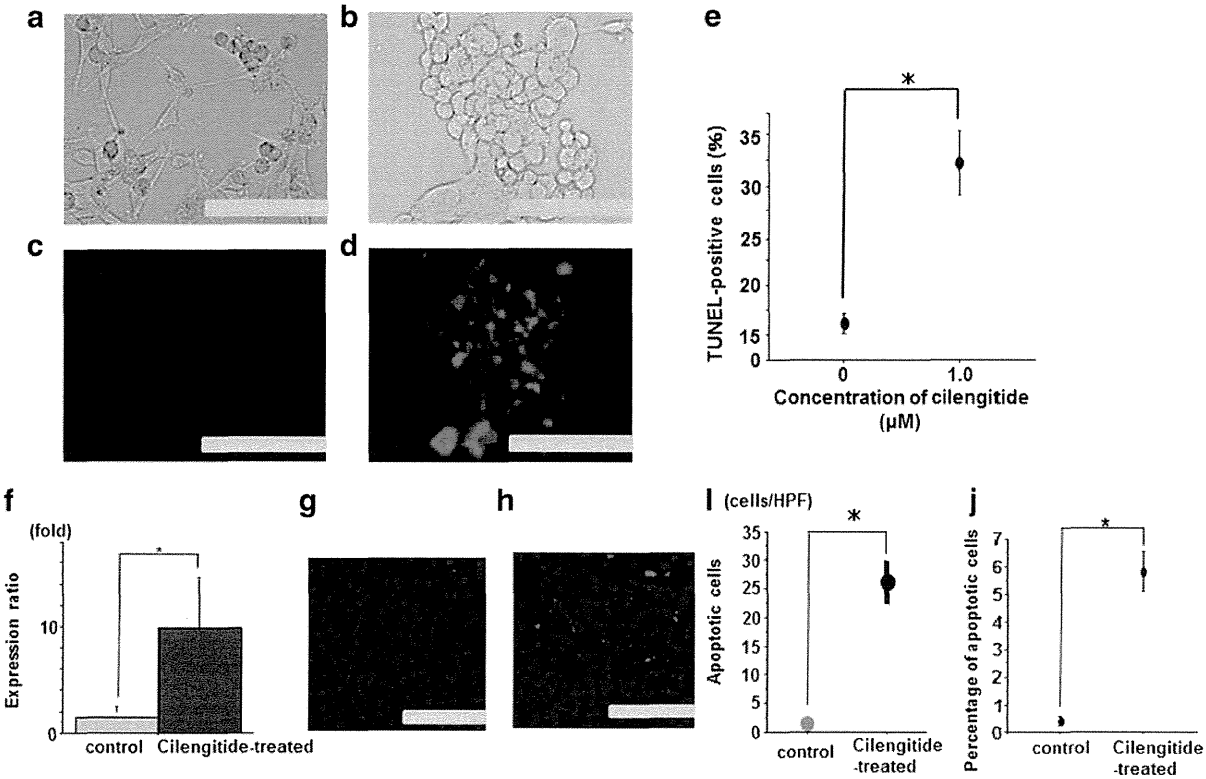

Figure 4 Nuclear DNA fragmentation in cilengitide-treated cells and in U87ΔEGFR-derived xenografts. To confirm the apoptosis of deformed glioma cells treated with cilengitide, the cells were stained with the In Situ Cell Death Detection Kit using TMR red. U87ΔEGFR cells in culture were composed of bipolar cells (**a**). They become spherical and agglutinated when cilengitide (1.0 μM) was added to their culture medium. Some of these deformed cells detached from the plate (**b**). Untreated U87ΔEGFR cells were negative (**c**), whereas U87ΔEGFR cell clusters treated with cilengitide were positive (**d**) (scale bar: 100 μm). The number of apoptotic cells in cilengitide-treated cells was significantly larger than in control. (*P < 0.05) (**e**). QRT-PCR analysis of cilengitide-treated caspase 8 gene expression in tumors treated with PBS or cilengitide. * P .007 (**f**) (mean ± SE, n 4) A subpopulation of apoptotic cells was visualized by TUNEL treatment (apoptotic cells: TMR red; nuclei: DAPI, blue) of U87ΔEGFR control xenografts (**g**) and U87ΔEGFR cilengitide-treated xenografts (**h**) (Scale bar 100 μm). The control sections exhibited scattered red fluorescence, whereas more punctate red fluorescence was observed in the cilengitide-treated xenografts. To quantify the cytotoxic effect of cilengitide, the number or percentage of apoptotic cells per high-power field (HPF) in U87ΔEGFR control xenografts and U87ΔEGFR cilengitide-treated xenografts was assessed. The number (**i**) or percentage (**j**) of apoptotic cells in cilengitide-treated xenografts was significantly larger than in control xenografts (*P < 0.05) (mean ± SE, n 5).

2000). Previously, we described the anti-invasive effect of cilengitide as its direct effect on glioma cells (Onishi et al. 2012) And we also reported the multiple mechanism of cilengitide for malignant glioma (Kurozumi et al. 2012).

Recent studies have shown that various cells are dependent on integrin-mediated adhesion to specific ECM proteins for their growth and survival and that detachment induces a form of apoptotic cell death recognized as anoikis (Chatterjee et al. 2000; Hynes 2002; Oliveira-Ferrer et al. 2008; Alghisi et al. 2009). Other studies reported that cilengitide exerts direct cytotoxic effects on glioma cells via an as yet unknown mechanism (Mikkelsen et al. 2009; Maurer et al. 2009; Oliveira-Ferrer et al. 2008). In this study, we examined the mechanism of cilengitide-induced cytotoxicity in glioma cells.

Microarray analysis

U87ΔEGFR cells were chosen for gene chip analysis because they have a more aggressive phenotype than other cell lines. ΔEGFR confers enhanced tumorigenicity on glioblastoma cells through elevated proliferation and reduced apoptotic rates *in vivo*. It will be important and interesting if we conduct a newly found cell death signaling pathway via integrin stimulation in this aggressive cell line.

Our data using the most sophisticated DNA microarray to date, profiling over 57000 genes, revealed the mechanism underlying the anti-glioma effect of cilengitide. After cilengitide treatment of glioma cells, apoptosis-related genes (i.e., caspase 8, desmoplakin, and protein kinase C, zeta) were upregulated. Apoptotic cleavage of

cellular proteins, FasL/CD95L signaling, TNF receptor signaling pathway, and ceramide signaling pathway were included in the significantly enriched molecular pathways.

Apoptosis is regulated by a series of biochemical events that commit a cell to death. A common feature of cells undergoing apoptosis is the activation of caspases, a family of aspartic acid-directed proteases (Alnemri et al. 1996). Caspases are activated during apoptosis and cleave specific proteins, resulting in the irreversible commitment to cell death. The signal transduction proteins MEKK1, p21-activated kinase 2, and focal adhesion kinase are caspase substrates that contribute to the cell death response when cleaved.

FasL (CD95L) is a tumor necrosis factor (TNF)-related type II membrane protein (Suda et al. 1993). Fas (CD95) is a cell surface protein belonging to the TNF receptor superfamily, and is expressed in glioma cells (Husain et al. 1998). The binding of FasL to Fas induces the trimerization of Fas, and FADD (Fas associated via DD (death domain))/MORT1 binds to the trimerized FAS cytoplasmic region through the interaction of their respective DDs. Caspase-8 is then recruited to FADD/MORT1 through binding of the DED (dead effector domain) domains, which in turn may induce the self-activation of the protease domain (Nagata 1997).

TNF-R1-bound TRADD (TNF-receptor associated via DD) recruits FADD through DD interaction. In turn, FADD recruits procaspase-8 or -10, which are activated by proximity, via its DED. Protein kinase C, zeta, is also involved in the TNF receptor signaling pathway. Activation of caspase-8 and -10 is sufficient to initiate a signaling cascade that induces apoptosis (Schneider-Brachert et al. 2004).

Recently, similar changes in human umbilical vein endothelial cells (HUVECs) have been reported for S 36578-2, a novel RGD mimetic that selectively activates the αvβ3 and αvβ5 integrins(Maubant et al. 2006). This compound induces cell detachment and apoptosis by the direct activation of caspase-8. Aoudjit and Vuori (Aoudjit & Vuori 2001) reported that detachment-induced cell death in HUVECs resulted from the activation of the Fas pathway by FasL/Fas interaction, Fas-FADD complex formation, and caspase-8 activation. Previous reports on epithelial cells also documented the involvement of FADD and caspase-8 in detachment-induced apoptosis (Alghisi et al. 2009; Hynes 2002). Using human glioma cell lines expressing the αvβ3 and αvβ5 integrins, cilengitide caused a profound detachment and increase of apoptosis in glioma cells similar to what was observed in endothelial cells, suggesting that identical mechanisms might occur in both cell types (Oliveira-Ferrer et al. 2008).

Clinical application of cilengitide for malignant glioma

There have been several reports on the preliminary results of phase I and II trials of cilengitide for recurrent or newly diagnosed malignant glioma. Cilengitide monotherapy or combination treatment with radiation and/or temozolomide is well tolerated and exhibits modest antitumor activity (Reardon et al. 2008a; Reardon et al. 2008b; Nabors et al. 2012). According to our results, in addition to the anti-angiogenic and anti-invasion effects of cilengitide(Kurozumi et al. 2012; Onishi et al. 2012), the cytotoxic effect of cilengitide was clearly shown. cilengitide inhibited integrin binding and activated caspase-8. This caspase-8 activation effect of cilengitide would enhance the effect of other cytotoxic therapies. Several preclinical studies have shown an enhanced antitumor effect of cilengitide when administered in combinatorial therapeutic regimens (Burke et al. 2002; Abdollahi et al. 2005; Tentori et al. 2008; Reardon et al. 2008a). Mikkelsen et al. demonstrated that cilengitide dramatically amplified the efficacy of radiation therapy in an animal glioma model (Mikkelsen et al. 2009). Kurozumi et al. demonstrated the enhanced therapeutic efficacy of an oncolytic virus on experimental glioma following pretreatment with cilengitide (Kurozumi et al. 2007).

Conclusion

We showed the cytotoxic effect of cilengitide on glioma cells. Microarray analysis revealed the detailed mechanism of the cytotoxic effect of cilengitide. Cilengitide, an inhibitor of integrins, activated caspase-8 and induced apoptosis-related pathways.

Competing interests

The authors declare that they have no competing interests.

Authors' contributions

MO contributed to the experimental design, data collection, data analysis, data interpretation, and drafted the manuscript. KK initiated the project, data interpretation and drafted the manuscript. HM and YS carried out the Western blot analysis. KF carried out the activity assay of caspase. JI carried out the QRT-PCR for in vivo. TI and ID participated data interpretation, and helped draft the manuscript. EAC and BK participated in planning the study. All authors read and approved the final manuscript.

Acknowledgements

We thank H. Wakimoto, M. Arao, and A. Ishikawa for their technical assistance. This study was supported by grants-in-aid for Scientific Research from the Japanese Ministry of Education, Culture, Sports, Science, and Technology to K.K. (No. 20890133; No. 21791364), and T.I. (No. 19591675; No. 22591611).

Author details

[1]Department of Neurological Surgery, Okayama University Graduate School of Medicine, Dentistry and Pharmaceutical Sciences, 2-5-1, Shikata-cho, Kita-ku, Okayama 700-8558, Japan. [2]Department of Physiology, Okayama University Graduate School of Medicine, Dentistry and Pharmaceutical Sciences, Okayama, Japan. [3]Brigham and Women's Hospital, Neurosurgery, Boston, MA, USA. [4]Department of Neurological Surgery, Dardinger Laboratory for Neuro-oncology and Neurosciences, The Ohio State University, Columbus, OH, USA.

Received: 19 December 2012 Accepted: 4 April 2013
Published: 15 April 2013

References

Abdollahi A, Griggs DW, Zieher H, Roth A, Lipson KE, Saffrich R, Grone HJ, Hallahan DE, Reisfeld RA, Debus J, Niethammer AG, Huber PE (2005) Inhibition of alpha(v)beta3 integrin survival signaling enhances antiangiogenic and antitumor effects of radiotherapy. Clin Cancer Res 11 (17):6270–6279. doi:10.1158/1078-0432.CCR-04-1223

Albert JM, Cao C, Geng L, Leavitt L, Hallahan DE, Lu B (2006) Integrin alpha v beta 3 antagonist Cilengitide enhances efficacy of radiotherapy in endothelial cell and non-small-cell lung cancer models. Int J Radiat Oncol Biol Phys 65(5):1536–1543. doi:10.1016/j.ijrobp.2006.04.036

Alghisi GC, Ponsonnet L, Ruegg C (2009) The integrin antagonist cilengitide activates alphaVbeta3, disrupts VE-cadherin localization at cell junctions and enhances permeability in endothelial cells. PLoS One 4(2):e4449. doi:10.1371/journal.pone.0004449

Alnemri ES, Livingston DJ, Nicholson DW, Salvesen G, Thornberry NA, Wong WW, Yuan J (1996) Human ICE/CED-3 protease nomenclature. Cell 87(2):171. doi: S0092-8674(00)81334-3

Aoudjit F, Vuori K (2001) Matrix attachment regulates Fas-induced apoptosis in endothelial cells: a role for c-flip and implications for anoikis. J Cell Biol 152 (3):633–643

Brooks PC, Clark RA, Cheresh DA (1994a) Requirement of vascular integrin alpha v beta 3 for angiogenesis. Science 264(5158):569–571

Brooks PC, Montgomery AM, Rosenfeld M, Reisfeld RA, Hu T, Klier G, Cheresh DA (1994b) Integrin alpha v beta 3 antagonists promote tumor regression by inducing apoptosis of angiogenic blood vessels. Cell 79(7):1157–1164. doi:0092-8674(94)90007-8

Burke PA, DeNardo SJ, Miers LA, Lamborn KR, Matzku S, DeNardo GL (2002) Cilengitide targeting of alpha(v)beta(3) integrin receptor synergizes with radioimmunotherapy to increase efficacy and apoptosis in breast cancer xenografts. Cancer Res 62(15):4263–4272

Chatterjee S, Matsumura A, Schradermeier J, Gillespie GY (2000) Human malignant glioma therapy using anti-alpha(v)beta3 integrin agents. J Neurooncol 46(2):135–144

Friedlander M, Brooks PC, Shaffer RW, Kincaid CM, Varner JA, Cheresh DA (1995) Definition of two angiogenic pathways by distinct alpha v integrins. Science 270(5241):1500–1502

Hodivala-Dilke KM, Reynolds AR, Reynolds LE (2003) Integrins in angiogenesis: multitalented molecules in a balancing act. Cell Tissue Res 314(1):131–144. doi:10.1007/s00441-003-0774-5

Husain N, Chiocca EA, Rainov N, Louis DN, Zervas NT (1998) Co-expression of Fas and Fas ligand in malignant glial tumors and cell lines. Acta Neuropathol 95 (3):287–290

Hynes RO (2002) Integrins: bidirectional, allosteric signaling machines. Cell 110 (6):673–687. doi:S0092867402009716

Ichii O, Otsuka S, Namiki Y, Hashimoto Y, Kon Y (2011) Molecular pathology of murine ureteritis causing obstructive uropathy with hydronephrosis. PLoS One 6(11):e27783. doi:10.1371/journal.pone.0027783PONE-D-11-14494

Kambara H, Okano H, Chiocca EA, Saèki Y (2005) An oncolytic HSV-1 mutant expressing ICP34.5 under control of a nestin promoter increases survival of animals even when symptomatic from a brain tumor. Cancer Res 65(7):2832–2839. doi:10.1158/0008-5472.CAN-04-3227

Kurozumi K, Tamiya T, Ono Y, Otsuka S, Kambara H, Adachi Y, Ichikawa T, Hamada H, Ohmoto T (2004) Apoptosis induction with 5-fluorocytosine /cytosine deaminase gene therapy for human malignant glioma cells mediated by adenovirus. J Neurooncol 66(1–2):117–127

Kurozumi K, Hardcastle J, Thakur R, Yang M, Christoforidis G, Fulci G, Hochberg FH, Weissleder R, Carson W, Chiocca EA, Kaur B (2007) Effect of tumor microenvironment modulation on the efficacy of oncolytic virus therapy. J Natl Canc Inst 99(23):1768–1781. doi:10.1093/jnci/djm229

Kurozumi K, Ichikawa T, Onishi M, Fujii K, Date I (2012) Cilengitide treatment for malignant glioma: current status and future direction. Neurol Med Chir (Tokyo) 52(8):539–547. doi:DN/JST.JSTAGE/nmc/52.539

Leavesley DI, Ferguson GD, Wayner EA, Cheresh DA (1992) Requirement of the integrin beta 3 subunit for carcinoma cell spreading or migration on vitronectin and fibrinogen. J Cell Biol 117(5):1101–1107

MacDonald TJ, Taga T, Shimada H, Tabrizi P, Zlokovic BV, Cheresh DA, Laug WE (2001) Preferential susceptibility of brain tumors to the antiangiogenic effects of an alpha(v) integrin antagonist. Neurosurgery 48(1):151–157

Maubant S, Saint-Dizier D, Boutillon M, Perron-Sierra F, Casara PJ, Hickman JA, Tucker GC, Van Obberghen-Schilling E (2006) Blockade of alpha v beta3 and alpha v beta5 integrins by RGD mimetics induces anoikis and not integrin-mediated death in human endothelial cells. Blood 108(9):3035–3044. doi:10.1182/blood-2006-05-023580

Maurer GD, Tritschler I, Adams B, Tabatabai G, Wick W, Stupp R, Weller M (2009) Cilengitide modulates attachment and viability of human glioma cells, but not sensitivity to irradiation or temozolomide in vitro. Neuro Oncol 11 (6):747–756. doi:10.1215/15228517-2009-012

Michiue H, Tomizawa K, Matsushita M, Tamiya T, Lu YF, Ichikawa T, Date I, Matsui H (2005a) Ubiquitination-resistant p53 protein transduction therapy facilitates anti-cancer effect on the growth of human malignant glioma cells. FEBS Lett 579(18):3965–3969. doi:10.1016/j.febslet.2005.06.021

Michiue H, Tomizawa K, Wei FY, Matsushita M, Lu YF, Ichikawa T, Tamiya T, Date I, Matsui H (2005b) The NH2 terminus of influenza virus hemagglutinin-2 subunit peptides enhances the antitumor potency of polyarginine-mediated p53 protein transduction. J Biol Chem 280(9):8285–8289. doi:10.1074/jbc.M412430200

Mikkelsen T, Brodie C, Finniss S, Berens ME, Rennert JL, Nelson K, Lemke N, Brown SL, Hahn D, Neuteboom B, Goodman SL (2009) Radiation sensitization of glioblastoma by cilengitide has unanticipated schedule-dependency. Int J Cancer 124(11):2719–2727. doi:10.1002/ijc.24240

Nabors LB, Mikkelsen T, Rosenfeld SS, Hochberg F, Akella NS, Fisher JD, Cloud GA, Zhang Y, Carson K, Wittemer SM, Colevas AD, Grossman SA (2007) Phase I and correlative biology study of cilengitide in patients with recurrent malignant glioma. J Clin Oncol 25(13):1651–1657. doi:10.1200/JCO.2006.06.6514

Nabors LB, Mikkelsen T, Hegi ME, Ye X, Batchelor T, Lesser G, Peereboom D, Rosenfeld MR, Olsen J, Brem S, Fisher JD, Grossman SA (2012) A safety run-in and randomized phase 2 study of cilengitide combined with chemoradiation for newly diagnosed glioblastoma (NABTT 0306). Cancer. doi:10.1002/cncr.27585

Nagata S (1997) Apoptosis by death factor. Cell 88(3):355–365. doi:S0092-8674(00)81874-7

Narita Y, Nagane M, Mishima K, Huang HJ, Furnari FB, Cavenee WK (2002) Mutant epidermal growth factor receptor signaling down-regulates p27 through activation of the phosphatidylinositol 3-kinase/Akt pathway in glioblastomas. Cancer Res 62(22):6764–6769

Oliveira-Ferrer L, Hauschild J, Fiedler W, Bokemeyer C, Nippgen J, Celik I, Schuch G (2008) Cilengitide induces cellular detachment and apoptosis in endothelial and glioma cells mediated by inhibition of FAK/src/AKT pathway. J Exp Clin Cancer Res 27:86. doi:10.1186/1756-9966-27-86

Onishi M, Ichikawa T, Kurozumi K, Fujii K, Yoshida K, Inoue S, Michiue H, Chiocca EA, Kaur B, Date I (2012) Bimodal anti-glioma mechanisms of cilengitide demonstrated by novel invasive glioma models. Neuropathology. doi:10.1111/j.1440-1789.2012.01344.x

Reardon DA, Fink KL, Mikkelsen T, Cloughesy TF, O'Neill A, Plotkin S, Glantz M, Ravin P, Raizer JJ, Rich KM, Schiff D, Shapiro WR, Burdette-Radoux S, Dropcho EJ, Wittemer SM, Nippgen J, Picard M, Nabors LB (2008a) Randomized phase II study of cilengitide, an integrin-targeting arginine-glycine-aspartic acid peptide, in recurrent glioblastoma multiforme. J Clin Oncol 26(34):5610–5617. doi:10.1200/JCO.2008.16.7510

Reardon DA, Nabors LB, Stupp R, Mikkelsen T (2008b) Cilengitide: an integrin-targeting arginine-glycine-aspartic acid peptide with promising activity for glioblastoma multiforme. Expert Opin Investig Drugs 17(8):1225–1235. doi:10.1517/13543784.17.8.1225

Schneider-Brachert W, Tchikov V, Neumeyer J, Jakob M, Winoto-Morbach S, Held-Feindt J, Heinrich M, Merkel O, Ehrenschwender M, Adam D, Mentlein R, Kabelitz D, Schutze S (2004) Compartmentalization of TNF receptor 1 signaling: internalized TNF receptosomes as death signaling vesicles. Immunity 21(3): 415–428. doi:10.1016/j.immuni.2004.08.017S1074761304002341

Stupp R, Weber DC (2005) The role of radio- and chemotherapy in glioblastoma. Onkologie 28(6-7):315–317. doi:10.1159/000085575

Suda T, Takahashi T, Golstein P, Nagata S (1993) Molecular cloning and expression of the Fas ligand, a novel member of the tumor necrosis factor family. Cell 75(6):1169–1178. doi:0092-8674(93)90326-L

Tentori L, Dorio AS, Muzi A, Lacal PM, Ruffini F, Navarra P, Graziani G (2008) The integrin antagonist cilengitide increases the antitumor activity of temozolomide against malignant melanoma. Oncol Rep 19(4):1039–1043

Tucker GC (2003) Alpha v integrin inhibitors and cancer therapy. Curr Opin Investig Drugs 4(6):722–731

Varner JA, Cheresh DA (1996a) Integrins and cancer. Curr Opin Cell Biol 8(5):724–730. doi:S0955-0674(96)80115-3

Varner JA, Cheresh DA (1996b) Tumor angiogenesis and the role of vascular cell integrin alphavbeta3. Important Adv Oncol:69–87

Varner JA, Emerson DA, Juliano RL (1995) Integrin alpha 5 beta 1 expression negatively regulates cell growth: reversal by attachment to fibronectin. Mol Biol Cell 6(6):725–740

Xiong JP, Stehle T, Diefenbach B, Zhang R, Dunker R, Scott DL, Joachimiak A, Goodman SL, Arnaout MA (2001) Crystal structure of the extracellular segment of integrin alpha Vbeta3. Science 294(5541):339–345. doi:10.1126/science.10645351064535

Yoshino K, Motoyama S, Koyota S, Shibuya K, Usami S, Maruyama K, Saito H, Minamiya Y, Sugiyama T, Ogawa J (2011) IGFBP3 and BAG1 enhance radiation-induced apoptosis in squamous esophageal cancer cells. Biochem Biophys Res Commun 404(4):1070–1075. doi:10.1016/j.bbrc.2010.12.115

doi:10.1186/2193-1801-2-160
Cite this article as: Onishi *et al.*: Gene expression profiling of the anti-glioma effect of Cilengitide. *SpringerPlus* 2013 2:160.

Brain Tumor Pathol (2013) 30:34–39
DOI 10.1007/s10014-012-0093-1

ORIGINAL ARTICLE

Measurement and cellular sources of the soluble interleukin-2 receptor in primary central nervous system lymphoma

Ryuhei Kitai · Hirohito Sasaki · Ken Matsuda · Kenzo Tsunetoshi · Takahiro Yamauchi · Hiroyuki Neishi · Kazuki Matsumura · Akira Tsunoda · Hiroaki Takeuchi · Kazufumi Sato · Ken-ichiro Kikuta

Received: 30 November 2011 / Accepted: 22 February 2012 / Published online: 8 March 2012

Abstract The aims of this study were to determine the diagnostic utility of the serum levels of the soluble interleukin 2 receptor (sIL-2R) as a tumor marker of primary central nervous system lymphoma (PCNSL) and to investigate the cellular source of sIL-2R using immunohistochemical staining. The serum sIL-2R levels of 37 samples from suspected PCNSL patients were measured. There were 13 patients with PCNSL and 24 patients with other diseases such as glioma, metastatic tumor, inflammation, or cerebrovascular disease. The serum sIL-2R levels of the PCNSL cases and other brain diseases were 629.5 ± 586.0 U/ml (mean ± SD; range 189–2220 U/ml) and 408.5 ± 250.7 U/ml (160–837 U/ml), respectively. The serum sIL-2R levels of the two groups overlapped, and hence the difference between them was not significant. sIL-2R is the α subunit of IL-2R. It is also known as CD25, and is cleaved from its position in the cell membrane and released into the blood. CD25 expression was immunohistochemically detected in 7 of 11 PCNSL samples. Confocal laser microscopy revealed that CD25 signals were present in atypical cells and mononuclear cells. We concluded that both lymphoma cells and infiltrating T cells express CD25, which is one of the cellular sources of sIL-2R.

Keywords Primary CNS lymphoma · CD25 · sIL-2R

R. Kitai (✉) · H. Sasaki · K. Matsuda · K. Tsunetoshi · T. Yamauchi · H. Neishi · K. Matsumura · A. Tsunoda · H. Takeuchi · K. Sato · K. Kikuta
Department of Neurosurgery, Faculty of Medical Sciences, University of Fukui, Fukui, Japan
e-mail: kitai@u-fukui.ac.jp

Introduction

In the WHO classification of brain tumors, PCNSL is defined as a malignant lymphoma arising in the CNS in the absence of any obvious lymphoma outside of the nervous system at the time of diagnosis, and its incidence has recently increased markedly [1]. Although modern neuroimaging of the central nervous system is advantageous for the differential diagnosis of brain tumors, it still remains difficult to distinguish PCNSL from other brain diseases in some cases [1, 2]. Brain biopsy sampling remains the gold standard in all patients unless surgical procedures are contraindicated.

The serum levels of the soluble IL-2 receptor (sIL-2R) have been used as a tumor marker of hematological malignancies, and those of patients with aggressive non-Hodgkin's lymphoma have been reported to be more than ten times higher than those of healthy controls [3–5]. The majority of PCNSLs are non-Hodgkin's lymphomas such as diffuse large B-cell lymphoma [1]. However, the sIL-2R levels of PCNSL patients have not been well studied [6]. It was reported that increased levels of sIL-2R indicate T lymphocyte activation [6, 7]. sIL-2R is not unique to T cells, but rather is also expressed on HTLV-1 transformed T and B cells, EBV transformed B cells, myeloid precursors, and oligodendrocytes [3, 7]. It is absent from resting T cells, non-activated B cells, and null cells [3, 7]. Histologically, reactive T lymphocytes and monohistiocytic cells have been found within PCNSL tissue [8]. The purpose of this study was to retrospectively reassess the diagnostic value of sIL-2R in suspected PCNSL patients and to immunohistochemically investigate the type of cells that produce sIL-2R in PCNSL specimens.

Materials and methods

We reviewed the medical records of patients that were initially suspected to be suffering from PCNSL at our institute from 2007 to 2011. Nineteen were male, and 18 were female (Tables 1, 2). The age of the patients ranged from 19 to 90 years of age (mean 61.7 years). The patients had undergone systemic surveillance, including physical examinations; blood and serum analysis including analyses of sIL-2R and C-reactive protein (CRP); and computed tomography of the neck, chest, abdomen, and pelvis, where necessary. According to the patients' final diagnoses, the sIL-2R levels of 13 PCNSL cases, 14 cases of other CNS tumors, 3 cases of inflammation, and 7 cases of cerebrovascular disease were retrospectively investigated.

The patients' serum sIL-2R levels were determined by a commercial laboratory company using the sandwich enzyme-linked immunosorbent assay. In 11 of the 13 PCNSL cases formalin-fixed paraffin-embedded PCNSL specimens were collected from our archives. The other two cases of PCNSL were diagnosed according to the cytological features of their cerebrospinal fluid. A histological diagnosis of malignant lymphoma was agreed on among the authors in all cases.

Immunohistochemistry and confocal laser microscope analysis

Immunohistochemical staining was performed according to the manufacturer's protocol. Primary antibodies against CD45 (leukocyte common antigen; DAKO M0701; 1:100), CD20 (B cell marker; DAKO M0755; 1:100), CD3 (T cell marker; Spring Bioscience M3070; 1:200), and CD25 (IL-2R α subunit; Novocastra NCL-CD25-305; 1:100) were used. For antigen retrieval, tissue sections were boiled in 10 mM citrate buffer for 10 min. Negative controls were produced by treating parallel sections using the above method but without the primary antibody. The staining procedure was achieved using the Envision plus technique (DAKO, Japan).

The cellular source(s) of sIL-2R were assessed by immunohistochemical staining using a confocal laser microscope equipped with an Ar/Kr/HeNe laser combination laser (Leica TCS SP: Leica Microsystems, Germany). Rhodamine-labeled (TAGO, CA, USA; 1:100) secondary antibodies for CD25 and 4′,6-diamidino-2-phenylindole (DAPI) for nuclear staining were also used.

Table 1 Clinical and laboratory data and immunohistochemical detection of CD25 in PCNSL

Case	Age (years)	Sex	sIL-2R (U/ml)	CRP (mg/dl)	CD25 immunoreactivity of specimen
1	59	M	189	0.39	Negative
2	81	M	695	0.71	Atypical cells, mononuclear cells
3	56	M	2220	0.79	Atypical cells
4	52	F	197	0.03	Negative
5	81	F	445	0.01	Atypical cells, mononuclear cells
6	74	M	390	0.06	Negative
7	78	F	357	<0.10	*1
8	75	F	258	<0.10	Atypical cells, mononuclear cells
9	65	M	1525	0.19	Mononuclear cells
10	67	F	452	0.02	Atypical cells
11	62	F	459	<0.10	Negative
12	56	F	572	0.1	Mononuclear cells
13	90	M	425	1.13	*1

*1 diagnosed by cerebrospinal fluid and neuroimaging

Table 2 Clinical and laboratory data and final diagnosis of suspected PCNSL

Case	Age (years)	Sex	sIL-2R (U/ml)	CRP (mg/dl)	Final diagnosis
14	76	M	254	0.25	ICH (subacute phase)
15	42	F	207	0.01	GBM
16	76	F	650	0.12	Cerebral infarction
17	48	F	246	0.04	Metastasis (cardiac myxoma)
18	50	M	277	0.1	Metastasis (unknown origin)
19	29	M	376	<0.02	Multiple sclerosis
20	63	M	836	0.28	Anaplastic astrocytoma
21	58	M	310	0.03	Atypical meningioma
22	76	F	335	<0.02	Cerebellar infarction
23	76	M	250	0.09	Aspergillosis
24	58	M	394	0.02	Brain stem glioma
25	66	M	308	0.04	Spinal cord tumor
26	25	M	160	0.54	Cystic vestibular schwannoma
27	70	F	529	0.12	Metastasis (lung cancer)
28	58	M	416	<0.02	Hemangioblastoma
29	58	F	212	<0.10	Anaplastic astrocytoma
30	23	M	263	<0.10	GBM
31	19	F	241	<0.10	Multiple sclerosis
32	72	M	331	0.14	Cerebral infarction
33	44	F	307	ND	Meningioma
34	68	M	398	1.28	ICH (subacute phase)
35	80	F	857	3.52	Hemorrhagic infarction
36	76	F	387	1.97	Anaplastic astrocytoma
37	75	F	516	2.32	GBM

ICH intracerebral hemorrhage, *GBM* glioblastoma multiform, *ND* not determined

Statistical analysis

Serological data were analyzed using the Mann-Whitney *U* test and a computer system.

Results

Serological results

The 13 PCNSL cases showed elevated levels of sIL-2R (629.5 ± 586.0 U/ml, range 189–2220 U/ml), whereas the other disease group showed sIL-2R levels of 408.5 ± 250.7 U/ml (range 160–837 U/ml). The difference between the groups was not statistically significant. As elevated serum levels of sIL-2R have been reported in a variety of autoimmune and inflammatory diseases [3, 7], the cases with serum CRP levels of greater than 1 mg/ml were excluded to avoid the influence of inflammation. As a result, one case of PCNSL and five cases of other diseases were excluded (Tables 1, 2). The mean sIL-2R level of the remaining 12 PCNSL samples was 646.0 ± 609.1 U/ml, which was significantly higher than that of the other disease group (347.0 ± 166.6 U/ml; $p = 0.025$; Mann-Whitney *U* test). There was a large overlap between the sIL-2R values of the two groups (Fig. 1).

Pathological results

The surgical PCNSL specimens showed typical compact cellular aggregates with an angiocentric infiltration pattern. The immunohistochemical staining of CD20 confirmed that all of the PCNSL cases examined in this study were B cell type lymphoma. CD3 positive T cells were seen in all specimens, but the extent of cell infiltration differed from case to case. Immunohistochemical analysis showed that CD25 was expressed on the membranes of both neoplastic cells and mononuclear cells in the PCNSL sections (Fig. 2a, b). Five of the 11 PCNSL specimens contained CD25-positive atypical cells. Two specimens only displayed CD25-positive mononuclear cells, which were considered to be infiltrating T cells. The intensity of the immunopositivity varied from case to case. Neither atypical cells nor CD25-positive mononuclear cells were observed in 4 of the 11 specimens. No CD25 positive cells were detected in normal brain tissue. To strengthen our data regarding the cellular source of CD25 in B cell lymphoma, we performed immunofluorescent staining and examined the specimens using a confocal laser scope. As shown in Fig. 3, CD25 signals (Rhodamine; red) were detected in the cell membranes of the lymphoma cells. Overlaid images produced with the double staining technique revealed that the CD25 signal was present in the cells with atypical nuclei. It was concluded that some lymphoma cells produce CD25.

A high serum sIL-2R level was noted in two patients (cases 1 and 9). Pathological specimens in two cases showed typical diffuse large B cell type lymphoma without any differences in the other nine cases.

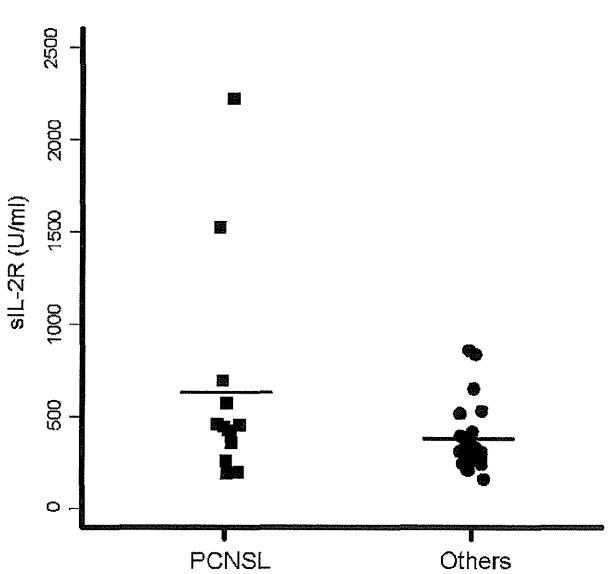

Fig. 1 Graph showing the serum sIL-2R levels in PCNSL and other diseases. *Bars* show mean values

A representative case with high serum sIL-2R

A 56-year-old man who had a history of glomerulonephritis and acute subdural hematoma complained a progressive deterioration of higher brain functions (case 3). Fluid-attenuated inversion recovery (FLAIR)-MRI revealed diffuse white matter hyperintensity involving the bilateral cerebral hemispheres, corpus callosum, and white matter adjacent to the posterior horn of lateral ventricles (Fig. 4). Gadolinium was not administered because of renal dysfunction. The serum sIL-2R level was elevated to 2,220 U/ml (normal range 145–518 U/ml). The biopsy specimen revealed typical PCNSL as diffuse large B-cell lymphoma. The tumor cells were strongly labeled by antibodies for CD20, a B cell marker (Fig. 4). The patient was treated with corticosteroids and whole brain irradiation involving a total dose of 40 Gy. After the completion of radiotherapy, the value of sIL-2R was decreased according to the tumor shrinkage. Then, the patient relapsed, and the sIL-2R level was elevated. He died 4 months after the initial presentation.

Discussion

Magnetic resonance (MR) imaging of immunocompetent PCNSL patients typically demonstrates one or more

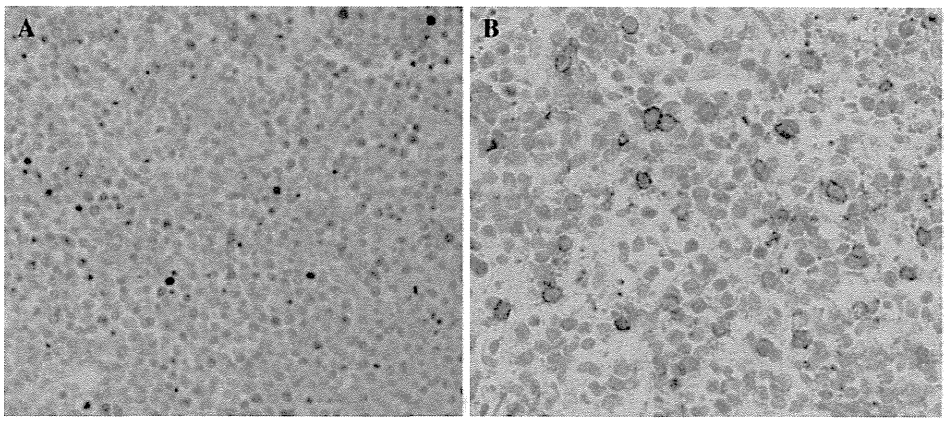

Fig. 2 **a** Infiltrating mononuclear cells showed positivity for CD25 (case 2). **b** Immunohistochemical staining of PCNSL tissue revealed that atypical large cells were positive for CD25 (case 8)

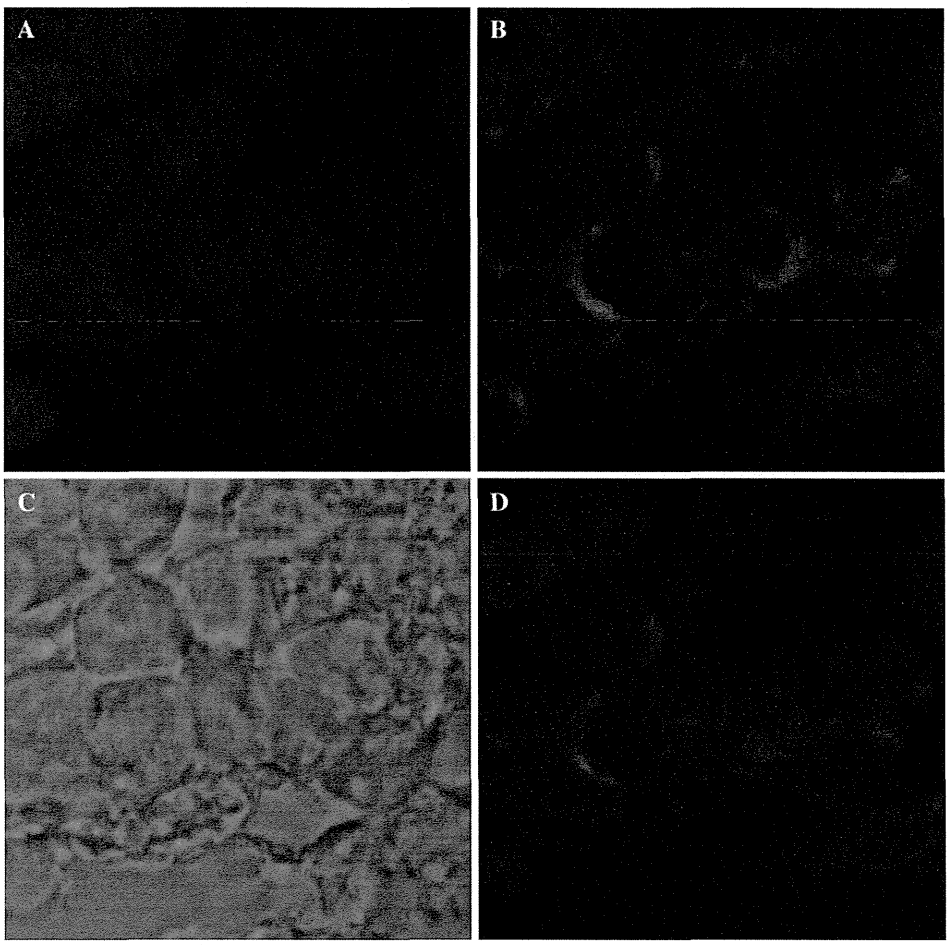

Fig. 3 Double staining observations by confocal laser imaging: **a** DAPI nuclear staining, **b** rhodamine red staining of CD25, **c** phase contrast image, **d** superimposition of **a** and **b** revealing tumor cells that expressed CD25 (case 10)

homogeneously enhanced lesions in the periventricular white matter [1, 2]. After neuroimages suggestive of PCNSL are obtained, a minimally invasive diagnostic procedure is recommended [2, 6, 8]. Establishing new non-surgical diagnostic tools for PCNSL would be helpful. The serum sIL-2R level was reported to be significantly high in

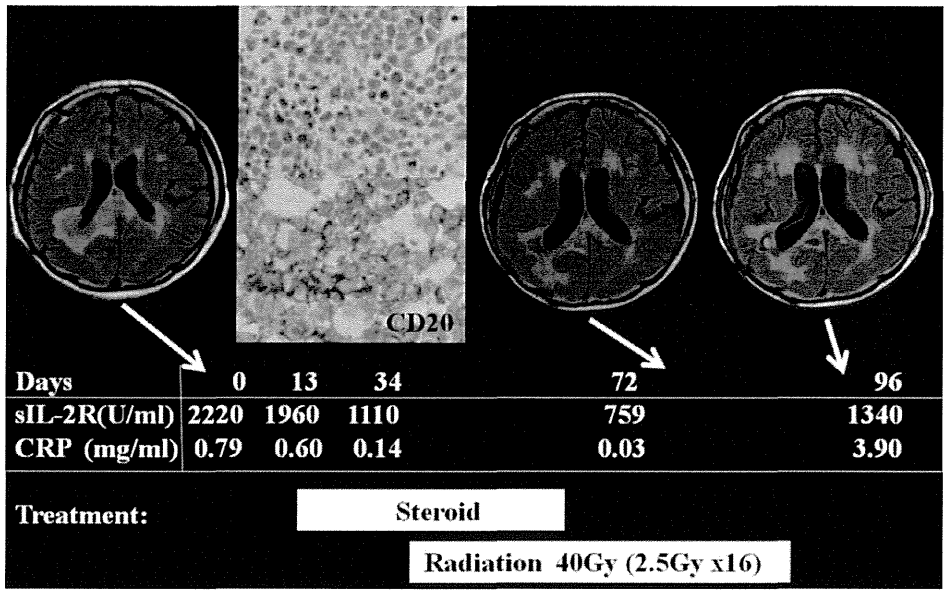

Fig. 4 Clinical course in case 3. The value of sIL-2R decreased during corticosteroid administration and radiation therapy. Abnormal intensity lesions in FLAIR-MRI decreased in size (*left* and *middle* MRI). The surgical specimen showed typical PCNSL. Note that the periventricular lesion was enlarged at tumor relapse (*right* MRI)

highly aggressive lymphomas and was subsequently recognized to reflect the tumor burden and indicate a poor outcome [4, 5, 7]. Although sIL-2R is easy to measure, there have been few studies of the sIL-2R level in PCNSL [6].

IL-2 was discovered as a T-cell proliferative factor that was purified from cultured phytohemagglutinin-stimulated peripheral blood mononuclear cells [9]. The IL-2 receptor is expressed on the cell membranes of lymphocytes and plays important roles in their activation and proliferation [3, 7, 10]. The cell surface-bound IL-2R is composed of three glycoprotein chains: α (55 kDa), β (75 kDa), and γ (64 kDa) chains. Most resting T cells, B cells, and monocytes in the circulation do not express the α subunit [10]. Expression of the α chain, which is also known as CD25, is rapidly induced after mononuclear cell activation, whereas the β and γ chains are constitutively expressed by the above-mentioned cells [3, 7]. The release of the α subunit into the blood is proportional to its cell surface expression. After its release, the α subunit is excreted and catabolized by the kidneys and has a serum half-life of 0.62 h [3]. If CD25 is only found on neoplastic cells and is released directly into the blood; it follows that the serum level of sIL-2R directly reflects the burden of malignantly transformed cells and disease activity. In other words, sIL-2R could be used as a true neoplastic marker. In our study, the serum sIL-2R levels of the two groups often overlapped, and the IL-2 levels of the two groups were not significantly different. The serum levels of sIL-2R are known to increase during various immunological and inflammatory processes [3, 7, 11]. CRP and sIL-2R might be regulated differently in various inflammatory conditions [11, 12]. After we had excluded cases displaying elevated CRP levels, our data indicated that the serum sIL2R levels of PCNSL patients were significantly higher than those of patients with other diseases. However, the PCNLS patients showed a wide range of sIL-2R values, and so it is not a sensitive and specific marker. This variation was thought to have been caused by the presence of several cases with abnormally high levels of sIL-2R. Our data showed that extremely high levels of sIL-2R (>1500 U/ml) were only observed in PCNSL patients. In contrast, the cases lacking the surface CD25 antigen displayed a relatively low level of sIL-2R. Thus, high sIL-2R levels without inflammatory disease might be suggestive of PCNSL. However, pathological specimens in higher sIL-2R cases failed to show any differences compared to lower sIL-2R cases.

The precise source and biological role of sIL-2R in PCNSL has not been clarified [6]. sIL-2R is reported to be released by systemic Hodgkin's lymphomas or systemic lymphomas that constitutively express the CD25 antigen on their membranes [3, 7]. This study revealed that sIL-2R was derived from the tumor cells themselves in some PCNSL cases. Activated lymphoid cells that had infiltrated neoplastic tissues also expressed CD25. Several studies have shown that not only lymphoid cancer cells, but also some non-lymphoid cancer cells express IL-2R on their surfaces [3, 5, 10]. They include carcinomas of the kidney, head and neck, esophagus, and lung [3]. In addition, the elevated levels of sIL-2R observed in some malignant solid tumors are likely to have been released from normal peripheral mononuclear cells that were activated in response to the neoplasm's growth or from activated lymphoid cells that had infiltrated neoplastic tissues.

Overall, serum sIL-2R is not a specific and highly sensitive marker of PCNSL. As shown in Fig. 4, the serial evaluation of sIL-2R might be useful in monitoring of therapeutic effectiveness. Further studies are needed to find a more specific marker for this type of lymphoma.

Acknowledgments This study was partially supported by Grant-in-Aid for Scientific Research no. 23592118.

References

1. Louis DN, Ohgaki H, Wiestler OD et al (2007) Malignant lymphomas. WHO classification of tumours of the central nervous system, 4th edn. IARC, Lyon, pp 188–192
2. Jack CR, Reese DF, Scheithauer BW (1985) Radiographic findings in 32 cases of primary CNS lymphoma. AJNR 6:899–904
3. Bien E, Balcerska A (2008) Serum soluble interleukin 2 receptor alpha in human cancer of adults and children: a review. Biomarkers 13:1–26
4. Ennishi D, Yokoyama M, Terui Y et al (2009) Soluble interleukin-2 receptor retains prognostic value in patients with diffuse large B-cell lymphoma receiving rituximab plus CHOP (RCHOP) therapy. Ann Oncol 20:526–533
5. Shimomura Y, Tsurumi H, Sawada M et al (1999) Clinical significance of serum soluble interleukin-2 receptor level in patients with non-Hodgkin's lymphoma. Rinsho Ketsueki 40:639–645
6. Fujimaki T (2010) Tumor markers for primary central nervous system lymphomas. Nihon Rinsho 68:289–291
7. Rubin LA, Nelson DL (1990) The soluble interleukin-2 receptor: biology, function, and clinical application. Ann Intern Med 113:619–627
8. Kitai R, Ishisaka K, Sato K et al (2007) Primary central nervous system lymphoma secretes monocyte chemoattractant protein 1. Med Mol Morphol 40:18–22
9. Morgan DA, Ruscetti FW, Gallo R (1976) Selective in vitro growth of T lymphocytes from normal human bone marrows. Science 193:1007–1008
10. Takeshita T, Asao H, Ohtani K (1992) Cloning of the gamma chain of the human IL-2 receptor. Science 257:379–382
11. Alenius GM, Eriksson C, Rantapää Dahlqvist S (2009) Interleukin-6 and soluble interleukin-2 receptor alpha-markers of inflammation in patients with psoriatic arthritis? Clin Exp Rheumatol 27:120–123
12. Pereira FO, Frode TS, Medeiros YS (2006) Evaluation of tumour necrosis factor alpha, interleukin-2 soluble receptor, nitric oxide metabolites, and lipids as inflammatory markers in type 2 diabetes mellitus. Mediators Inflamm 2006:1–7

Brain Tumor Pathol (2013) 30:104–108
DOI 10.1007/s10014-012-0112-2

CASE REPORT

Coincident choroid plexus carcinoma and adrenocortical tumor in an infant

Kazuhiko Yoshida · Kazufumi Sato · Ryuhei Kitai · Norichika Hashimoto · Toshihiko Kubota · Ken-Ichiro Kikuta

Received: 21 January 2012 / Accepted: 15 June 2012 / Published online: 1 July 2012

Abstract We report a case of a 20-month-old girl with a large choroid plexus carcinoma arising in the left lateral ventricle and an adrenocortical tumor. Following brain tumor resection, the patient was treated with radiation and chemotherapy. The adrenocortical tumor was found with the manifestation of precocious puberty. *TP53* gene mutation (exons 4–10) was not detected in either specimen. The patient had leptomeningeal dissemination and died 26 months later.

Keywords Choroid plexus carcinoma · Adrenocortical tumor · Malignancy

Introduction

Choroid plexus tumors are relatively uncommon intraventricular neoplasms of neuro-ectodermal origin, accounting for less than 1 % of all intracranial tumors. Most cases occur in children under 2 years of age [1, 2]. Choroid plexus carcinoma (CPC) is even rarer, representing no more than 25 % of all plexus tumors [3–7]. Some choroid plexus malignant tumors are associated with adrenocortical tumors [8–11]. We herein report the case of an infant with no known family history of malignancies who presented with two primary tumors, CPC and a benign adrenal cortical adenoma.

K. Yoshida (✉) · K. Sato · R. Kitai · N. Hashimoto · T. Kubota · K.-I. Kikuta
Department of Neurosurgery, Faculty of Medical Sciences, University of Fukui, 23-3, Shimoaizuki, Eiheiji-cho, Fukui 910-1193, Japan
e-mail: yoshidam@peach.plala.or.jp; ky239623@go.mitene.or.jp

Case report

A 20-month-old girl was admitted because of a 3-week history of gradual progression of occasional vomiting and right hemiparesis. Magnetic resonance imaging (MRI) revealed a 7-cm-diameter mass with contrast enhancement in the atrium of the left lateral ventricle (Fig. 1a) and a 1-cm-diameter mass in the interpeduncular fossa. Cerebral angiography revealed a small tumor blush, which was mainly fed by the left anterior and posterior choroidal arteries. The infant's prenatal and natal histories were of no significance. There was no family history of malignancies. Through left posterio-parietal craniotomy, the patient underwent tumor excision two times during 3 weeks. However, the tumor mass was only partially excised owing to profuse bleeding and brain swelling. For the purpose of reducing the vascularity and size of the tumor, a total dose of 32 Gy of irradiation was given to the limited area of the residual tumor over 4 weeks. The tumor mass regressed on MRI, and the central part of the tumor showed decreased contrast enhancement, which was interpreted as necrosis (Fig. 1b). Subsequently, gross total removal of the tumor in the left lateral ventricle was successfully performed (Fig. 1c), and her right hemiparesis gradually improved. A ventriculo-peritoneal shunt was placed to relieve hydrocephalus.

Histologically, the surgical specimens in the initial operation were characterized by papillary and tubular structures lined by single or multiple layered epithelia (Fig. 2a). Nuclear pleomorphism and necrosis were found (Fig. 2b). Five or more mitotic figures were seen per 10 HPF (Fig. 2b), and the Ki-67 labeling index was 12 % (DAKO, M7240, Fig. 2c). Immunohistochemical reactivity was positive against transthyretin (DAKO, L1857, Fig. 2d), cytokeratin (45- and 52-kd cytokeratin, YLEM,

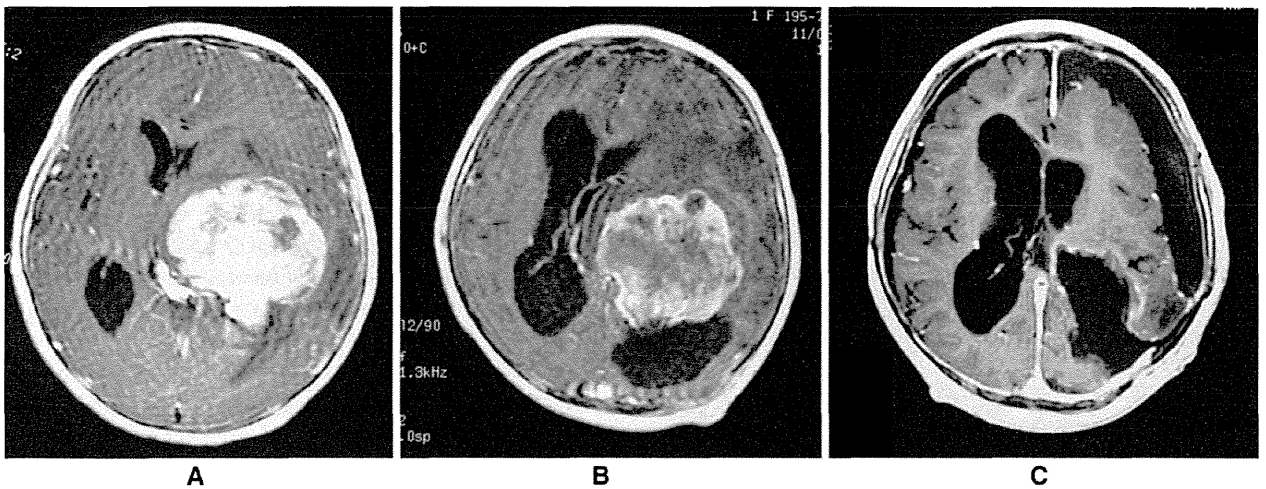

Fig. 1 **a** Axial T_1-weighted magnetic resonance images with gadolinium showing a large tumor in the left lateral ventricle. **b** Gadolinium-enhanced T1-weighted magnetic resonance image following irradiation to the tumor, showing noticeable diminution in enhancement. **c** Postoperative gadolinium-enhanced T_1-weighted magnetic resonance image showing total tumor excision in the left lateral ventricle

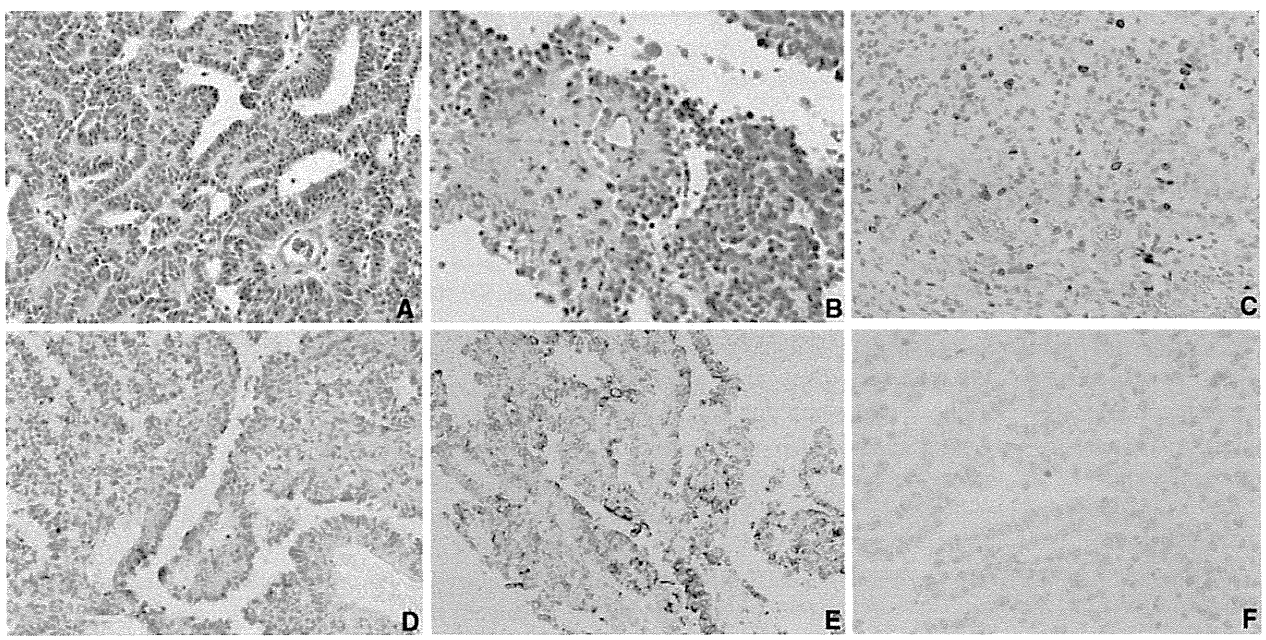

Fig. 2 **a** A photomicrograph of the tumor showing papillary and tubular structures lined by single or multiple layered epithelia with hypercellularity. HE stain, original magnification ×200. **b** A photomicrograph of the tumor showing nuclear pleomorphsim and necrotic area. HE stain, original magnification ×400. **c** A photomicrograph of the tumor showing the Ki-67 labeling index is 12 %. Original magnification ×200. **d** A photomicrograph of immunohistochemical staining showing cytoplasmic positivity for transthyretin (TTR). TTR immunoperoxidase, original magnification ×200. **e** A photomicrograph of immunohistochemical staining showing positivity for cytokeratin. Original magnification ×200. **f** A photomicrograph of immunohistochemical staining for p53 showing that few tumor cells were positive. Original magnification ×400

5D3, Fig. 2e), S-100 protein (DAKO, Z0311) and vimentin (DAKO, M0725), and was negative for glial fibrillar acid protein (GFAP, DAKO, Z0334), carcinoembryonic antigen (CEA, DAKO, A0115), epithelial membrane antigen (DAKO, M0613) and synaptophysin (DAKO, M0776). Immunohistochemical staining for p53 (DAKO, DO-7) revealed that few tumor cells were positive (Fig. 2f). Electron microscopically, numerous golf-club-shaped

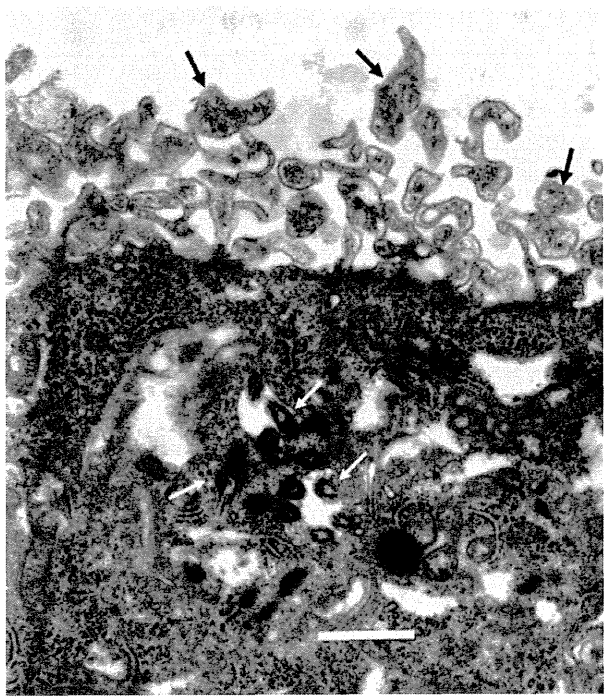

Fig. 3 An electron micrograph showing numerous golf-club-shaped microvilli (*black arrows*) on the luminal surface and cilia (*white arrows*) in the cytoplasm. *Bar* 1 μm

microvilli were demonstrated on the luminal surface. Cilia were occasionally seen in the cytoplasm (Fig. 3). A basement membrane was observed on their inner surface. All these histopathological findings were consistent with a diagnosis of CPC.

One month after the last operation, the patient developed signs of premature puberty such as pubic and axillary hair growth, hypertrophy of the clitoris and acne. Endocrinological studies revealed exceedingly high values of plasma testosterone at 3.3 ng/ml, the normal level being less than 0.1 ng/ml, and dehydroepiandrosterone-sulfate (DHEA-S) at 21,200 μg/dl, the normal range being 20–119 μg/dl. Abdominal MRI disclosed a large right adrenal mass 5.0 cm in diameter (Fig. 4a). The adrenal cortical tumor was entirely removed, producing immediate resolution of the patient's symptoms of premature puberty as well as normalization of the plasma levels of testosterone and DHEA-S. Histologically, the tumor consisted of neoplastic growth of atypical eosinophilic cells with a solid or alveolar growth pattern with moderate cellular pleomorphism. Mitotic figures were occasionally seen (1–2 per 10 HPF). No apparent necrosis or invasive growth was detected. Vascular invasion was inconspicuous (Fig. 4b). According to Weiss's criteria [12], our case was diagnosed as a benign adenoma. None of the adrenocortical tumor cells reacted to p53 antibody (Fig. 4c).

Genomic DNA was extracted from the paraffin blocks of the brain tumor and the adrenal tumor (TaKaRa DEXPAT, Takara, Kyoto, Japan), and also from her white blood cells. Amplification of the *TP53* gene within exons 4–10 was carried out with hot-start PCR polymerase (KOD-PLUS, Toyobo, Japan). Sequencing reaction (BigDye Terminator v1.1 Cycle Sequencing Kit, Applied Biosystems) was analyzed using a capillary sequencer (ABI PRISM 3100, Applied Biosystems). No mutation was detected in any of the DNA samples (exons 4–10) extracted from the specimens (Fig. 5).

MRI obtained 5 months after the last operation for the brain tumor disclosed leptomeningeal metastases. After additional radiation therapy and five cycles of chemotherapy including etoposide and carboplatin, tumor regression was observed. Nevertheless, she eventually succumbed to disseminated disease 26 months after the initial surgery.

Discussion

CPC is the malignant counterpart of choroid plexus tumors and histologically corresponds to WHO grade III [13]. This case fulfilled the following features: frequent mitosis, increased cellular density, nuclear pleomorphism, blurring of the papillary pattern with poorly structured sheets of tumor cells and necrotic area [13]. The differential diagnosis should include papillary ependymoma and metastatic papillary carcinoma, especially from the lung [5, 14]. Immunohistochemistry was positive for transthyretin, cytokeratin, S-100 protein and vimentin in the present case, but there was negative immunostaining for GFAP and CEA. Transthyretin and cytokeratin are reliable markers of choroid plexus neoplasms [15–17]. The expression of cytokeratin and transthyretin by tumor cells and the lack of GFAP expression differentiated this tumor from ependymoma, and the co-expression of cytokeratin, S-100 protein and vimentin with negative CEA was helpful in distinguishing it from metastatic carcinoma [13]. Electron microscopy favored the diagnosis of a choroid plexus tumor owing to the presence of golf-club-shaped microvilli, cilia and a basement membrane [18–20].

CPC in children generally follows an aggressive course [14], and the 5-year survival rate is 26–50 % [2, 3, 5, 6]. The tumor often disseminates via CSF pathways [5, 21], and even metastasizes extraneurally [22]. Previous reports confirm that maximum surgical resection offers the best chance for long-term survival. However, complete surgical excision cannot be carried out in all patients because of the extreme vascularity, larger size and its location [2–6]. To reduce the vascularity and volume of choroid plexus neoplasms, radiation therapy was beneficial in achieving complete resection [23–25].

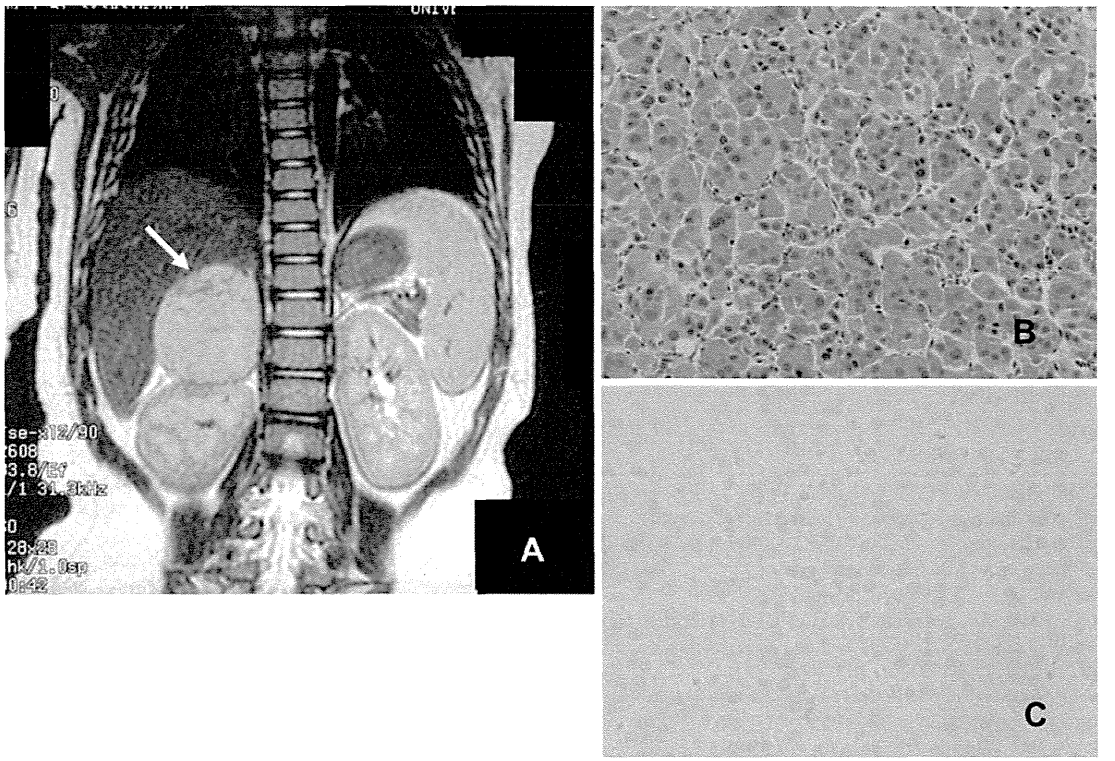

Fig. 4 **a** A coronal T_1-weighted magnetic resonance image showing a large right adrenal tumor (*arrow*). **b** A photomicrograph of the adrenal tumor showing neoplastic growth of atypical eosinophilic cells with a solid or alveolar growth pattern with moderate cellular pleomorphism. No apparent necrosis or invasive growth can be seen. HE stain, original magnification ×200. **c** A photomicrograph of immunohistochemical staining for p53 showing none of the tumor cells was positive. Original magnification ×400

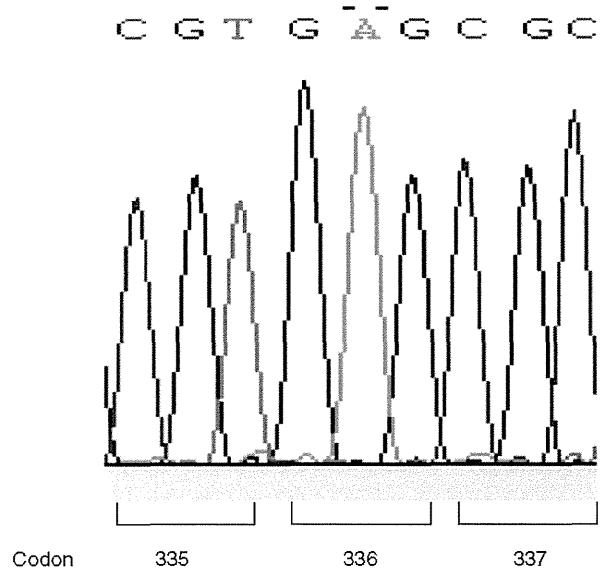

Fig. 5 One of the point mutation hotspots of *TP53* gene, codon 337 was judged to have no mutation

Childhood adrenocortical tumors (ACT) are very aggressive endocrine neoplasms whose incidence is quite low. According to the International Pediatric Adrenocortical Tumor Registry, they typically present during the first 5 years of life and have female predominance. Hormonal hyperproduction is almost universal, and most patients (84.2 %) present with virilization [26]. Pediatric ACT may occur sporadically or as a component of certain hereditary tumor syndromes, that is, Li–Fraumeni syndrome, multiple endocrine neoplasia type 1, Beckwith-Wiedmann syndrome, Carney complex and congenital adrenal hyperplasia [27].

Sandrini et al. [8] mentioned one pediatric case of combined CPC and adrenocortical carcinoma in 58 cases of childhood adrenocortical tumor. Vital et al. [9] reported a pediatric patient who had adrenocortical carcinoma at the age of 4 years, and the later atypical choroid plexus papilloma was discovered at 6 years, with p53 germline mutation in both tumors. In addition, Wang et al. described a boy aged 18 months who had coincident CPC and adrenocortical carcinoma with elevated p53 protein expression immunohistologically in both tumors [10]. More recently, Russell-Swetek et al. reported a young boy with no family history of cancer who was diagnosed with CPC and adrenocortical carcinoma, and harbored a novel de novo germline *TP53* mutation [11]. Thus, two of these reported cases are considered as Li–Fraumeni syndrome.

Since we failed to show *TP53* germline mutation in our case, this case is likely to be a rare coexistence of CPC and adrenocortical adenoma in an infant. However, both tumors are exceedingly rare; it is possible that the patient had other unknown genetic predispositions toward malignancy.

In conclusion, we should know this type of coincidence of tumors in infants.

References

1. Boyed MC, Steinbock P (1987) Choroid plexus tumors: problems in diagnostics and management. J Neurosurg 66:800–805
2. McEvoy A, Harding BN, Phipps KP et al (2000) Management of choroid plexus tumors in children: 20 years experience at a single neurosurgical centre. Pediatr Neurosurg 32:192–199
3. Berger C, Thiesse P, Lellouch TA et al (1998) Choroid plexus carcinomas in childhood: clinical features and prognostic factors. Neurosurgery 42:470–475
4. Packer RJ, Perilongo G, Johnson D et al (1992) Choroid plexus carcinoma of childhood. Cancer 69:580–585
5. Ellenbogen RG, Winston KR, Kupsky WJ (1989) Tumors of the choroid plexus in children. Neurosurgery 25:327–335
6. Pencalet P, Sainte RC, Lellouch TA et al (1998) Papillomas and carcinomas of the choroid plexus in children. J Neurosurg 88:521–528
7. Pierga JY, Kalifa C, Terrier-Lacombe MJ et al (1993) Carcinoma of the choroid plexus: a pediatric experience. Med Pediatr Oncol 21:480–487
8. Sandrini R, Ribero RC, DeLacerda L (1997) Childhood adrenocortical tumors. J Clin Endocrinol Metab 82:2027–2031
9. Vital A, Bringuier PP, Huang H et al (1998) Astrocytomas and choroids plexus tumors in two families with identical p53 germline mutations. J Neuropathol Exp Neurol 57:1061–1069
10. Wang L, Cornford ME (2002) Coincidental choroid plexus carcinoma and adrenocortical carcinoma with elevated p53 expression: a case report of a 18-month-old boy with no family history of cancer. Arch Pathol Lab Med 126:70–72
11. Russell-Swetek A, West AN, Mintern JE et al (2008) Identification of a novel TP53 germline mutation E285V in a rare case of paediatric adrenocortical carcinoma and choroid plexus carcinoma. J Med Genet 45:603–606
12. Weiss LM, Medeiros LJ, Vickery AL et al (1989) Pathologic features of prognostic significance in adrenocortical carcinoma. Am J Surg Pathol 13:202–206
13. Louis DN, Ohgaki H, Wiestler OD, et al (2007) Choroid plexus tumours. WHO Classification of Tumours of the Central Nervous System, 4 edn. Lyon, IARC, pp 82–85
14. Dohrmann GJ, Collias JC (1975) Choroid plexus carcinoma. Case report. J Neurosurg 43:225–232
15. Albrecht S, Rouah E, Becker LE et al (1991) Transthyretin immunoreactivity in choroid plexus neoplasms and brain metastasis. Mod Pathol 4:610–614
16. Ho DM, Wong TT, Liu HC (1991) Choroid plexus tumors in children. Histopathologic study and clinico-pathological correlation. Child's Nerv Syst 7:437–441
17. Newbould MJ, Kelsey AM, Arango JC et al (1995) The choroid plexus carcinomas of childhood: histopathology, immunocytochemistry and clinopathological correlations. Histopathol 26:137–143
18. Matsushima T (1983) Choroid plexus papillomas and human choroid plexus: a light and electron microscopic study. J Neurosurg 59:1054–1062
19. McComb RD, Burger PC (1983) Choroid plexus carcinoma: report of a case with immunohistochemical and ultrastructural observations. Cancer 51:470–475
20. Sato K, Hayashi M, Kubota T, et al (1989) A case of large malignant choroid plexus papilloma in the third ventricle-immunohistochemical and ultrastructural studies. No to Shinkei 41:973–978 (Jpn, with Eng abstract)
21. Ausman JI, Shrontz C, Chason J et al (1984) Aggressive choroid plexus papilloma. Surg Neurol 22:472–476
22. Valladares JB, Perry RH, Kalbag RM (1980) Malignant choroid plexus papilloma with extraneural metastasis. Case report. J Neurosurg 52:241–255
23. Carrea R, Polak M (1977) Preoperative radiotherapy in the management of posterior fossa choroid plexus papillomas. Child's Brain 3:12–24
24. Hawkins JC III (1980) Treatment of choroid plexus papillomas in children: a brief analysis of twenty year's experience. Neurosurgery 6:380–384
25. Wolff JEA, Sajedi M, Coppes MJ et al (1999) Radiation therapy and survival in choroid plexus carcinoma. Lancet 353:2126
26. Michalkiewicz E, Sandrini R, Figueiredo B et al (2004) Clinical and outcome characteristics of children with adrenocortical tumors: a report from the International pediatric Adrenocortical Tumor Registry. J Clin Oncol 22:838–845
27. Ribeiro RC, Figueiredo B (2004) Childhood adrenocortical tumours. Eur J Cancer 40:1117–1126

Ann Nucl Med (2013) 27:772–780
DOI 10.1007/s12149-013-0747-z

ORIGINAL ARTICLE

Analysis of progression and recurrence of meningioma using ^{11}C-methionine PET

Hidetoshi Ikeda · Naohiro Tsuyuguchi · Noritsugu Kunihiro · Kenichi Ishibashi · Takeo Goto · Kenji Ohata

Received: 31 January 2013 / Accepted: 16 June 2013 / Published online: 26 June 2013

Abstract
Objective The recurrence rate of meningioma after surgery is high, and progression is often observed. The risk factors for recurrence and progression are not clear. We evaluated the risk factors for recurrence and progression in meningioma using ^{11}C-methionine (MET) positron emission tomography (PET).
Methods Thirty-seven patients (mean follow-up, 80 months) with an intracranial meningioma were enrolled. MET PET was performed before treatment between 1995 and 2010, and patients were followed up in an out-patient clinic. Surgery was performed in 33 patients, and a wait-and-see approach was taken in four patients. We evaluated the extent of tumor resection, location, WHO grade, Ki-67 labeling index, and lesion to normal ratio (LN ratio) of MET uptake.
Results Six of the surgical cases had a recurrence, and two of the observation-only patients had tumor progression. A high LN ratio of MET uptake was a significant risk factor for recurrence and progression with univariate analysis. The area under the curve of receiver operating characteristic curve for the LN ratio of MET uptake was 0.754, and the optimal cutoff value was 3.18 (sensitivity 63 %, specificity 79 %). With multivariate analysis, a high LN ratio of MET uptake, non-gross total resection, and a high WHO grade were significant risk factors for progression and recurrence.
Conclusion A high LN ratio of MET uptake was a risk factor for tumor progression and recurrence. The advantage of MET PET is that it is not invasive and can easily be used to evaluate the whole tumor.

Keywords ^{11}C-methionine PET · Meningioma · Riskfactor of recurrence and progression · Multivariable analysis · ROC analysis

Introduction

Meningioma is the most common primary brain tumor in adults. The frequency of meningioma among all types of brain tumors is 26.4 % in Japan [1] and 34.4 % in the United States. Many histopathological subtypes exist. Most meningiomas are benign, but World Health Organization (WHO) grade II and grade III meningiomas, which exhibit aggressive clinical behavior, are found in 10 % of patients with meningioma. We usually perform surgery for symptomatic cases or cases with large tumors. For small and asymptomatic cases, a wait-and-see approach is taken. However, gross total resection (GTR) is difficult in some surgical cases because of the tumor location and invasion into the brain tissue and the venous sinus. The residual tumor often recurs with malignancy, making the patient's prognosis poor. Meningiomas that are only observed sometimes progress and require surgical resection. In previous papers, the recurrence rate after surgery was high. Even if the tumor is removed completely, the recurrence rate is between 7 and 32 %. After subtotal resection, the recurrence rate is between 19 and 50 % [2–4].

The risk factors for progression and recurrence in meningioma are not clear, and clarification of these factors is important for determining surgical indications and

H. Ikeda (✉) · N. Tsuyuguchi · N. Kunihiro · K. Ishibashi · T. Goto · K. Ohata
Department of Neurosurgery, Osaka City University Graduate School of Medicine, 1-4-3 Asahi-machi, Abeno-ku, Osaka 545-8585, Japan
e-mail: hide-i@med.osaka-cu.ac.jp

treatment strategies. We usually use the Ki-67 labeling index (LI) to evaluate the proliferative activity, but surgery is required to obtain a tissue specimen. Surgery is invasive for the patient, and evaluating the risk of recurrence with the Ki-67 LI is controversial because the tissue specimen sometimes does not reflect the whole tumor.

In this study, we evaluated ^{11}C-methionine (MET) uptake of the whole tumor using MET positron emission tomography (PET) to investigate the risk factors for recurrence and progression.

Methods

Patients

From a database of patients who were examined with MET PET, we retrospectively retrieved data for all 73 patients who were diagnosed with intracranial meningioma between 1995 and 2010. These cases were not a consecutive series. We could not examine MET PET results for all meningioma cases because the number of cases that could be examined by MET PET per week in our facilities is limited. Thirty-seven patients fulfilled the inclusion criteria for this study: (1) patients were initially diagnosed with meningioma; (2) MET PET was performed before surgery or observation; (3) patients were followed at Osaka City University Hospital or affiliated hospitals; (4) during the follow-up period, no additional treatment was performed other than the first surgery. Thirty-three patients were excluded because of recurrence after surgery, and three patients dropped out during the follow-up period. Thus, 37 cases (23 females and 14 males) were enrolled in this study (Fig. 1). The mean age of the patients was 54.5 ± 12.9 years. All study participants provided informed consent, and the study design was approved by an ethics review board.

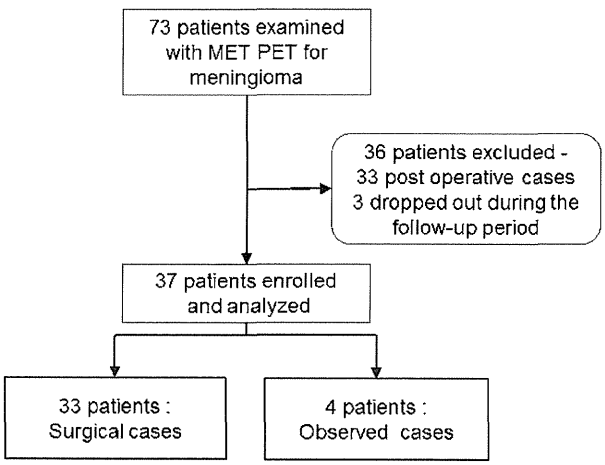

Fig. 1 Analysis of meningioma cases with MET PET

MET PET study

All patients underwent a MET PET scan with HEADTOME-IV (BGO, Shimadzu, Japan) between 1995 and 2005, Eminence-B (BGO) since 2005, and Biograph-16 (LSO, Siemens, Germany) since 2010. Twenty-six patients were examined with HEADTOME-IV. Axial and in-plane resolutions of the PET images were each 4.5 mm (in full width at half maximum), and the slice thickness was 4 mm. Twenty minutes after MET injection (4 MBq/kg), an emission scan of the brain was performed for 10 min. The emission scan was reconstructed to a matrix of 128 × 128 (using an iterative algorithm), and attenuation and scatter correction were done. The voxel size was 2 × 2 × 3.25 mm.

Ten patients were examined with Eminence-B. Axial and transaxial resolutions of the PET were each 4.5 mm (in full width at half maximum). The injection volume and timing of the scan were the same as HEADTOME-IV. The emission scan was reconstructed to a matrix of 128 × 128, and attenuation and scatter correction were done. The voxel size was 2 × 2 × 3.25 mm.

One patient was examined with Biograph-16. Axial and transaxial resolutions of the PET were 5.5 and 5.9 mm (in full width at half maximum), respectively. The injection volume and timing of the scan were the same as HEADTOME-IV. The emission scan was reconstructed to a matrix of 336 × 336, and attenuation and scatter correction were done. The voxel size was 1.02 × 1.02 × 2 mm.

All MET PET images were interpreted by an experienced neurosurgeon. The MET uptake was calculated by drawing a region of interest (ROI) using a freehand procedure. In all cases, MET uptake of the lesion was higher than in normal gray matter. In cases with a multiple meningioma, the lesion with the highest mass was evaluated. From the tumor lesion and normal reference region (frontal lobe of the normal side), the lesion to normal ratio (LN ratio) of mean MET uptake was calculated.

Surgical resection, pathological findings, and clinical follow-up

Thirty-three cases were treated with surgery, and four cases were observed. In surgical cases, GTR (Simpson grade I or II) was performed in 18 cases (55 %), and subtotal resection (Simpson grade III or IV) was performed in 13 cases (39 %). Partial resection (Simpson grade IV) was performed in one case (3 %), and a biopsy (Simpson grade V) was performed in one case (3 %). The pathological diagnosis and the WHO grade were determined by experienced

pathologists according to the WHO classification updated in 2007. The Ki-67 LI was also calculated. All patients were followed up at our out-patient clinic without any additional treatment for the tumor during the follow-up period. For the surgical cases, gadolinium (Gd)-enhanced magnetic resonance imaging (MRI) was performed every 3–6 months in the first 2 years after surgery, and then every year during the follow-up period. For the observation cases, Gd-enhanced MRI was performed more than once a year. The mean follow-up period was 80 ± 52 months (range 4–180 months). In surgical cases, the lesion was defined as a 'recurrence' when a lesion was found at the same location or a residual lesion was obviously enlarged in the radiological examinations. In non-surgical observation cases, the lesion was defined as a 'progression' when the tumor size was obviously enlarged in the radiological examinations.

We evaluated the risk factors for recurrence and progression by age, gender, location (skull base or not), extent of resection (GTR or not), Ki-67 LI, and LN ratio of MET uptake.

Statistical analysis

We evaluated the risk factors for recurrence and progression using paired t tests. When the data were not normally distributed, Wilcoxon's rank-sum test was used for continuous data. Fisher's exact tests were used for categorical data. Cox proportional hazards regression analysis was used for the surgical cases to assess the predictors of recurrence and progression with duration of the recurrence-free period as the time variable. A receiver operating characteristics (ROC) curve was assessed to confirm the best cutoff value of the LN ratio for recurrence and progression. All statistical analysis was performed using JMP 9 software (SAS Institute Inc.).

Results

Characteristics and pathology

During the follow-up period, six surgical patients had a recurrence, and two observation patients progressed. The characteristics of the 37 cases are shown in Table 1. Summaries of the recurrence group and the non-recurrence group are shown in Table 2. The mean age of the recurrence group was 57.9 ± 11.8 years, and that of the non-recurrence group was 53.6 ± 13.2 years. We found no significant difference in the numbers of males and females in each group.

The tumor location is shown in Table 1. We classified the tumor location into two groups: skull base and non-skull base. The recurrence rate was not significantly different between these two groups.

Two patients died during the clinical follow-up period. One (case 20) died of thyroid cancer 51 months after PET examination, and another (case 21) died due to tumor progression 4 months after PET examination. The tumors were classified by pathology as follows. Ten were meningothelial (30 %), nine were fibrous (27 %), eight were transitional (24 %), two were angiomatous (6 %), two were chordoid (6 %), one was secretory (3 %), and one was atypical (3 %). Thirty cases were WHO grade I meningiomas, and three cases were WHO grade II meningiomas. The recurrence rate was not significantly different between WHO grade I (17 %, 5/30 cases) and grade II (33 %, 1/3 cases). The mean LN ratio of WHO grade I meningiomas was 2.99 ± 1.07, and the mean LN ratio of WHO grade II meningiomas was 2.35 ± 0.36. The LN ratio was not significantly different between WHO grade I and grade II.

Extent of tumor resection and recurrence

Gross total resection was performed in 18 patients, and one patient (case 35) had a recurrence during clinical follow-up. In 15 patients, some tumor remained after the surgery. In this non-GTR group, recurrence of meningioma was observed in five patients. The recurrence rate was not significantly different between the non-GTR group and the GTR group ($p = 0.053$).

LN ratio of MET PET and Ki-67 LI for progression and recurrence

During the clinical follow-up, six cases of recurrence and two cases of progression were found. The average LN ratio of these eight cases was 3.67 ± 1.15 [95 % confidence interval (CI) 2.71–4.64] and that of the remaining 29 cases was 2.65 ± 0.86 (95 % CI 2.32–2.98). The average LN ratio of the cases with recurrence and progression was higher than that of the cases without recurrence or progression ($p < 0.01$, Fig. 2). The average Ki-67 LI of the recurrent six cases was 1.81 ± 1.21 (95 % CI 0.54–3.09), and that of the 27 cases without recurrence was 3.06 ± 3.84 (95 % CI 1.54–4.58). The Ki-67 LI was not significantly different between the recurrence group and the non-recurrence group ($p = 0.44$). No correlation was found between the LN ratio and the Ki-67 LI (Fig. 3). Risk factors evaluated with univariate analysis are summarized in Table 2. One illustrative case is shown in Fig. 4.

Table 1 Characteristics of 37 patients with meningioma

No.	Age (years)	Gender	Location	Pathological diagnosis	WHO grade	Ki-67	LN ratio	Surgery	Recurrence/ progression (months after pet exam)	Follow-up (months)
1	48	F	Parasagittal	Transitional	I	15.5	2.23	GTR	No	176
2	67	F	Parasagittal	Transitional	I	3	2.22	GTR	No	45
3	49	F	Sphenoid ridge	Chordoid	II	1.34	2.63	GTR	No	157
4	57	F	Petroclival	Secretory	I	14.4	3.00	GTR	No	40
5	49	M	Olfactory groove	Transitional	I	4.98	2.63	GTR	No	180
6	39	M	Pineal	Chordoid	II	3.03	1.95	GTR	No	26
7	61	F	Clival	Fibrous	I	4	5.10	STR	Yes (9)	141
8	43	M	Parasagittal	Fibrous	I	0.3	3.97	GTR	No	159
9	58	F	Parasagittal	Fibrous	I	1.45	3.10	GTR	No	34
10	46	F	Convexity	Fibrous	I	4.49	3.73	GTR	No	88
11	61	M	Clinoidal	Transitional	I	1.12	2.94	STR	No	152
12	79	M	Convexity	Meningothelial	I	1.26	5.38	STR	Yes (13)	56
13	57	F	Parasagittal	Angiomatous	I	2.29	3.61	STR	Yes (20)	147
14	37	F	Convexity	Meningothelial	I	2.27	3.37	GTR	No	145
15	54	F	Tentorial	Fibrous	I	0.59	3.32	STR	No	142
16	71	M	Parasagittal	Meningothelial	I	0.92	5.09	STR	No	65
17	66	F	C-P angle	Transitional	I	0.49	2.65	STR	No	138
18	22	F	Convexity	Meningothelial	I	1.3	1.98	GTR	No	130
19	60	M	Sphenoid ridge	Fibrous	I	1.33	2.90	STR	Yes (17)	71
20	74	M	Tuberculum sellae	Meningothelial	I	0.2	2.17	STR	No	51
21	39	M	Middle fossa	–	–		3.18	–	Yes (4)	4
22	75	F	C-P angle	Fibrous	I	3.5	2.35	GTR	No	54
23	52	F	Tuberculum sellae	Angiomatous	I	1	2.54	GTR	No	110
24	50	F	Sphenoid ridge	Meningothelial	I	1.26	1.65	STR	No	29
25	49	F	C-P angle	–	–	–	1.53	–	No	97
26	62	M	Convexity	Fibrous	I	3	2.86	STR	No	65
27	57	M	Convexity	Transitional	I	2.95	1.20	GTR	No	48
28	44	F	Foramen magnum	Meningothelial	I	5.6	2.64	GTR	No	48
29	48	F	Intraventricular	Fibrous	I	6.5	3.03	GTR	No	74
30	42	F	Sphenoid ridge	Transitional	I	2	2.73	STR	No	69
31	62	F	Convexity	Transitional	I	0.1	1.68	Biopsy	No	47
32	30	F	Intraventricular	–	–	–	2.49	–	No	24
33	69	F	Convexity	Meningothelial	I	0.3	1.27	GTR	No	43
34	49	M	Clivotentorial	–	–	–	2.39	–	Yes (43)	43
35	53	F	Intraventricular	Atypical	II	1.5	2.48	GTR	Yes (26)	26
36	65	M	Clival	Meningothelial	I	0.5	4.35	Partial	Yes (15)	25
37	72	M	Tentorial	Meningothelial	I	1	3.89	STR	No	23

C-P angle cerebello-pontine angle, *GTR* gross total resection, *STR* subtotal resection

In our study, the LN ratio was a significant risk factor for recurrence and progression with univariate analysis. We also evaluated risk factors using multivariate analysis. The results are summarized in Table 3. Multivariate analysis showed that the LN ratio, the extent of resection, and the WHO grade were significant risk factors for recurrence and progression. The hazard ratio of the LN ratio was 4.21. The LN ratio was the only factor examined preoperatively.

ROC curve analysis

A ROC curve was generated, and the area under the curve (AUC) was calculated to determine the best discriminating